

May 31st, 11:00 AM - 11:15 AM

Large Eddy Simulation of the water flow around a cylindrical pier mounted in a flat and fixed bed

P. X. Ramos
University of Porto

R. Maia
University of Porto

L. Schindfessel
Ghent University

T. De Mulder
Ghent University

J. P. Pêgo
University of Porto

Follow this and additional works at: <http://digitalcommons.usu.edu/ewhs>

 Part of the [Civil and Environmental Engineering Commons](#)

Ramos, P. X.; Maia, R.; Schindfessel, L.; De Mulder, T.; and Pêgo, J. P., "Large Eddy Simulation of the water flow around a cylindrical pier mounted in a flat and fixed bed" (2016). *International Junior Researcher and Engineer Workshop on Hydraulic Structures*. 3.
<http://digitalcommons.usu.edu/ewhs/2016/Session3/3>

This Event is brought to you for free and open access by the Conferences and Events at DigitalCommons@USU. It has been accepted for inclusion in International Junior Researcher and Engineer Workshop on Hydraulic Structures by an authorized administrator of DigitalCommons@USU. For more information, please contact dylan.burns@usu.edu.



Large Eddy Simulation of the water flow around a cylindrical pier mounted in a flat and fixed bed

P. X. Ramos^{1,2}, R. Maia¹, L. Schindfessel², T. De Mulder² and J. P. Pêgo¹

¹Dep. Civil Engineering
University of Porto – Faculty of Engineering
Porto, Portugal

²Hydraulics Laboratory
Dep. Civil Engineering – Ghent University
Ghent, Belgium

E-mail: pedro.ramos@ugent.be

ABSTRACT

In the present work, a numerical model based upon the Large Eddy Simulation approach has been set up for predicting the three-dimensional flow around a cylindrical pier, mounted on a flat and fixed bed, a generic case that is relevant for the study of flow and scour around bridge piers. This turbulent flow configuration was studied experimentally by Nogueira et al. (2008) with Particle Image Velocimetry (PIV). The main goal of this paper is a first validation of the numerical model, based upon the available data. The numerical tool is capable to qualitatively reproduce the characteristic flow features around the pier, like e.g. the horseshoe vortex system and the vortex shedding in the wake. The predicted extent of the initial scour hole, based upon the bed shear stress magnitudes, agrees well with the observations at the onset of the scouring process during the lab experiments. Further quantitative validation of the numerical model will benefit from additional measurement efforts in the experiments.

Keywords: CFD, LES, Ansys Fluent, cylindrical pier

1. INTRODUCTION

The flow past a circular cylinder is of practical relevance for many engineering fields, with regards to the flow around e.g. towers, chimneys, cables or bridge piers, with the latter being the subject of this work.

The flow disturbance caused by piers on riverbeds usually induces scour around those structures. The principal features of the corresponding flow pattern are shown in Figure 1. As the flow approaches the pier, its velocity decreases down to the point where the flow is halted at the upstream face of the obstacle. As a consequence of the change of the pressure field, an increment on the level of the free surface on the upstream side of the pier occurs, forming the so-called surface roller. Accordingly, the approach velocity is higher near the water surface than near the bed, as well as the pressure. Therefore, this pressure gradient results in a downflow that impinges on the bed and it is partially deflected upstream. Simultaneously, the boundary layer of the approaching flow undergoes a three-dimensional separation due to the adverse pressure gradient induced by the pier. The resulting horseshoe vortex is subsequently advected along both sides of the pier base. The aforementioned phenomena tend to scour the pier's foundation, both upstream and at the sides of the pier.

Scour around obstacles in rivers occurs after the formation of a scour cavity of sufficiently large dimensions to stabilize the large-scale oscillations of the horseshoe vortex (Kirkil and Constantinescu 2010). The latter dissipates itself downstream the pier, having an important role in the bed scour due to the bed material trailing (Melville and Coleman 2000).

At the lee side of the pier, the shedding of wake vortices can be seen. While the horseshoe vortex causes essentially the entrainment of the bed material, the wake vortices pluck the particles with a suction effect, transporting them then in suspension (Melville and Coleman 2000).

In summary, turbulent structures over a wide range of scales are present around the cylinder, controlling the entrainment and transport of sediment from the scour hole. Hence, to understand how the flow induces scour on the bed, it is necessary to properly account for the structure of the large-scale eddies around the cylinder.

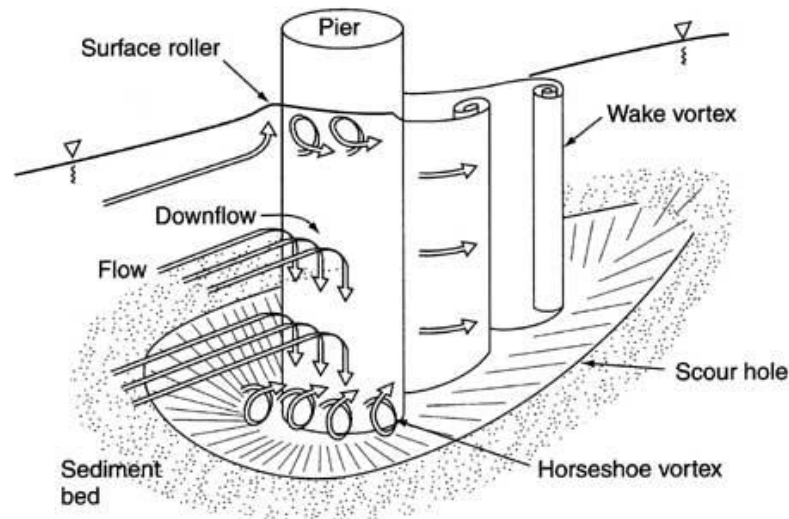


Figure 1. Flow pattern around a circular pier (Hammil 1999)

The flow around a circular cylinder has been extensively studied in fluid mechanics. For many years, due to the complexity of the flow structures involved, the study of this issue has been mostly experimental. Nevertheless, in the last decades, the numerical modeling of the flow around piers has been a growing field.

Thwaites (1960) reviewed the previous aerodynamic experimental studies about the flow around cylindrical structures. One of the earliest computational studies about flow around circular cylinders was conducted by Beaudan and Moin (1994). Nakamura et al. (1996) studied the vortex shedding from a rectangular pier both numerically and experimentally. Yulistiyanto et al. (1998) focused on the modeling of the flow over cylinder on shallow-water. Large Eddy Simulation (LES) was initially introduced for simulating atmospheric flows in the 1960s (Smagorinsky 1963) and has become one of the most successful methodologies for eddy-resolved modeling of turbulent flows (Zhiyin 2014). Researchers' attention has turned to the application of this model to flow around bluff bodies (e.g. Sakamoto et al. 1993, Yang et al. 1993, Murakami and Mochida 1995, Rodi et al. 1997, Franke and Frank 2002, Lisenko et al. 2012). Breuer (1998) studied the numerical and modeling influences on Large Eddy simulations for the flow past a circular cylinder. Catalano (2003) performed LES simulations of the flow around a circular cylinder at high *Reynolds* numbers. Kuroda et al. (2007) studied the flow around a rectangular cylinder (applying LES) and then compared the results with particle image velocimetry (PIV) data. Zhao and Huhe (2006) presented a 3D LES of the flow around a cylindrical pier.

Reviews of advances in the use of LES to study flow around bodies can be found in Zhiyin (2014), Majeed et al. (2015) and Schanderl and Manhart (2016), with the latter focused on the bed shear stress around a cylinder.

The hydrodynamic studies are important to understand and minimize the result of the deflection of the flow caused by the obstacle: scour. To understand scour around piers quantitative and qualitative data of the flow field are required. Although this subject has been extensively studied, some features of the flow are not fully understood. The body geometry is quite simple, but the flow structures around the body can be very complex, including separation with no fixed separation point, transition to turbulence in the thin shear layers, which are separating, and shedding of large scale vortices (Zdravkovich 1997). Nogueira et al. (2008) studied the flow around a cylindrical pier by means of PIV, showing the presence of the downflow and horseshoe vortex system upstream the cylindrical pier (schematized in Figure 1).

Although the main interest of the authors is scour around bridge piers, the primary goal of this paper is to assess the quality of an eddy-resolving numerical model based upon the LES approach for the flow field around a cylindrical pier in a flat fixed bed, representative for the initial phase of the scour process. More specifically, the objective is to simulate the flat bed lab experiments of Nogueira et al. (2008), allowing a partial validation of the numerical predictions. Additionally, validation data from literature will be used. This validation exercise is a first step towards numerical simulation of the scouring process and countermeasures (of cylindrical and even more complex bridge pier geometries).

Note that the use of the LES approach allows to reveal the dynamics of large-scale eddies in the flow around a circular pier, enabling the study of the influence of the flow structures on the bed shear stresses (which are difficult to measure in laboratory experiments) and on the cylinder itself. The bed shear stress values are useful to identify where and how scour will start to occur.

The outline of the paper is as follows. In section 2, the characteristics of the studied flow configuration will be described. Section 3 presents the numerical model set-up and verification criteria. Results on the instantaneous velocity fields, drag coefficient and bed shear stress are presented and discussed in section 4. Conclusions are drawn in section 5.

2. FLOW CONFIGURATION

As stated before, the reference case used for the numerical simulation is the experimental work of Nogueira et al. (2008), namely the configuration with a flat and fixed bed (Figure 2 and Table 1). The laboratory work was performed in a long water flume with 0.7 m width (B) and 8 m length. A PVC cylinder with 0.048 m diameter (D) was positioned and founded in the channel bed. The bed material consisted of quartz sand with a median diameter (d_{50}) equal to 0.837 mm with a coefficient of gradation (σ_D) equal to 1.48.



Figure 2. Experimental installation (from Nogueira et al. 2008)

Nogueira et al. (2008) also aimed at the study of the scour around the pier, measuring the scour cavity after 5 minutes (corresponding to 45 % of the equilibrium scour depth). The maximum depth of local scour is obtained for flow conditions near the critical condition ($U \approx U_c$), i.e. the mean flow velocity corresponds to the initiation of the particles' motion (Melville and Coleman 2000). Thus, the flow rate supplied (Q) was 20 l/s and the flow depth (h) equal to 0.10 m, resulting in a mean flow velocity of 0.286 m/s, a value which lies between the critical velocities suggested by Goncharov and Neil equations (Nogueira et al. 2008). The water temperature was kept around 20°C. Taking in consideration the features provided, the Reynolds number of the flow calculated based on the pier diameter is given by $Re_D = 1.37 \times 10^4$. The contraction and wall effects were negligible to the scouring process, since ratios of $B/D \geq 10$ and $B/h \geq 5$ (Moreno et al. 2012, Ramos et al. 2015) were guaranteed (see Table 1).

In accordance with the Shields diagram (Shields 1936), the critical shear stress of the bed particles is approximately 0.48 Pa. This parameter will be useful to compare with the bed shear stress values obtained in the numerical simulations.

Table 1. Characteristic parameters of experiment by Nogueira et al. 2008

d_{50} (mm)	B (m)	D (m)	B/D (-)	h (m)	B/h (-)	Q (m ³ /s)	U (m/s)	Re_D (-)
0.837	0.7	0.048	14.58	0.10	7.00	0.20	0.286	1.37×10^4

No measured data for the drag force on the pier are available in the data set of Nogueira et al. (2008). Therefore, use is made of information in the literature. The drag force on the pier depends on the *Reynolds* number. If the approaching flow were to be uniform over the flow depth, which is not the case in the experiment, the drag coefficient, C_D , is expected to oscillate around the mean value of 0.683 for $Re_D = 1.37 \times 10^4$ (Figure 5.3 of White 2006).

The oscillations of the drag force may (in principle) also be important to the pier's structural design, but this is beyond the scope of this paper. To quantify the shedding frequency of the wake vortices, no use can be made of measured velocities in the lee side of the pier, since they are absent in the data set of Nogueira et al. (2008). Therefore, again information in the literature will be relied upon. For a given main frequency, f , of the vortex shedding, the corresponding dimensionless *Strouhal* number, St (White 2006) is:

$$St = \frac{f \cdot D}{U} \quad (1)$$

where D is the diameter of the pier. For the present case, the *Strouhal* number according to literature (Figure 3) assumes a value of about 0.20. This yields a vortex shedding frequency of 1.19 Hz, hence a period (T) of 0.84 s.

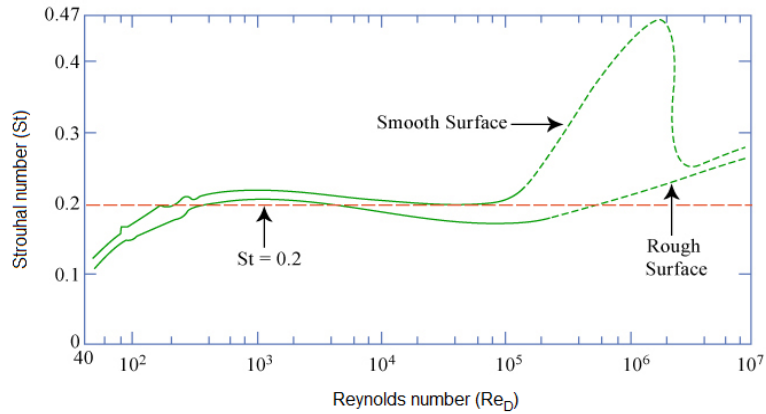


Figure 3. Relationship between *Strouhal* number and *Reynolds* number for circular cylinders, after Techet (2005), data from Lienhard (1966) and from Roshko (1955)

3. NUMERICAL MODEL

3.1. Computational mesh

A 3-D finite-volume incompressible Navier-Stokes model, applying the Large Eddy Simulation approach, is set up and run by means of the *Ansys Fluent* software. The mesh used for the simulations is a parallelepiped (0.7 m wide and 0.1 m high), representing the fluid domain, with a cylindrical cavity, with a diameter of 0.048 m, representing the pier (Figure 4). The geometric model is not very complex, allowing the adoption of a block-structured mesh with an O-grid mesh with a radius of $6D$ around the cylinder. The pier's zone was subjected to a further refinement (Figure 5 and Figure 6), as well as the cells next to the walls and bed. Note however, that the wall boundary layers are not fully resolved. In order to limit the computational time, a so-called wall model will be relied upon. In Figure 4, the sub-zones of the mesh are indicated. The grey arrows indicate the cell size gradient direction (from the smallest to the biggest cell). Note the smaller cells are next to the cylindrical pier and walls (Table 2). Also, a size cell gradient in the z -direction was applied (with the finer cells near the bed). Note that the presented mesh is the final result of some (iterative) mesh optimization efforts, aiming at mesh independency of the solution as well as respecting some quality criteria (see also 3.5).

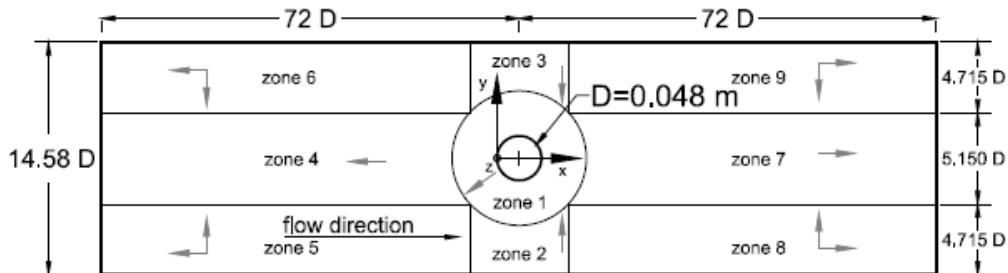


Figure 4. Computational domain with indication of the zones of the mesh and direction of the cell size grading (not to scale)

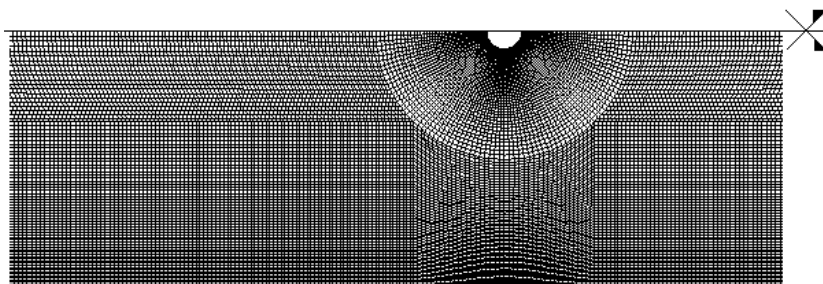


Figure 5. Partial plan view of the mesh (mesh is symmetric with respect to the x axis shown in Figure 4)

Table 2. Number of cells in each zone of the mesh

Zone of the mesh	x-direction		y-direction		z-direction	
	Size of first cell (mm)	Number of Cells	Size of first cell (mm)	Number of Cells	Size of first cell (mm)	Number of Cells
1	0.005	200	0.0025	100	0.015	80
2, 3	0.010	30	0.010	50	0.015	80
4	3.000	400	3.000	80	0.015	80
5, 6	0.010	400	0.010	60	0.015	80
7	3.000	300	3.000	80	0.015	80
8, 9	0.010	300	0.010	30	0.015	80

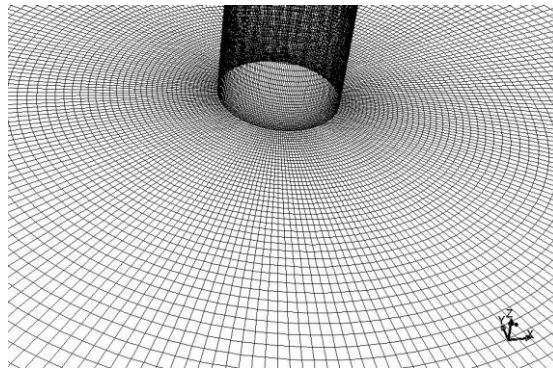


Figure 6. Detailed view of the mesh next to the pier

3.2. Boundary conditions

Taking advantage of the available PIV data regarding the approaching flow, the inlet boundary condition was defined by three velocity profiles at $y = 0.175$ m, $y = 0$ m (symmetry axis) and $y = -0.086$ m, respectively (i.e. points A, B and C of Figure 7), corresponding to the total discharge ($Q = 20$ l/s). According to the literature, the inlet distance from the pier ($72D$) is sufficient for the turbulence to be developed (Ferziger and Peric 2002). The standard wall model from *Fluent* (Lauder and Spalding 1974) was used to model the flow near the walls, bed and pier. In the outlet, the outflow condition from *Fluent* was applied, meaning a zero diffusion flux for all flow variables (the conditions of the outflow plane are extrapolated from within the domain and have no impact on the upstream flow) and an overall mass balance correction.

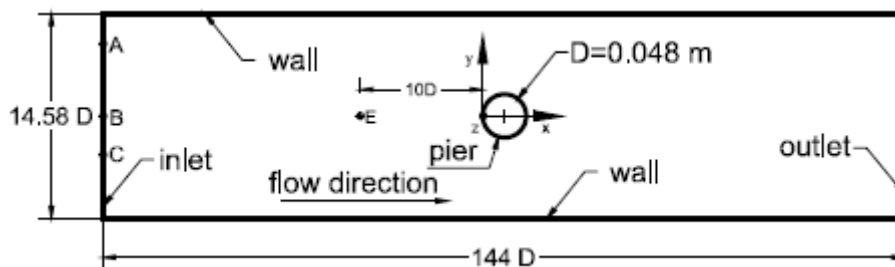


Figure 7. Schematic description of the domain (plan view) and its boundary-conditions (not to scale).

The upper boundary condition (water surface) was modelled by means of a rigid lid without any friction. As mentioned before (Section 1) and shown in Figure 8, in reality an elevation of the water level occurs upstream of the pier, a phenomenon which is accompanied by a surface roller.

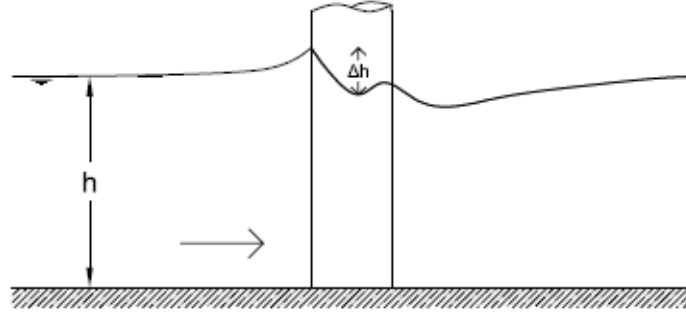


Figure 8. Schematic description of free-surface upstream the pier (Roulund et al. 2005).

The free surface elevation upstream the pier is a phenomenon mostly influenced by the *Froude* number of the flow (Roulund et al. 2005). The higher the *Froude* number, the bigger is the described effect. For relatively small *Froude* numbers, Δh (i.e. the difference between the water level immediately upstream the pier and the lowest point of the water surface close to the pier) is given by Equation 2 (Roulund et al. 2005).

$$\frac{\Delta h}{h} = \frac{Fr^2}{2} \quad (2)$$

In the present case, the *Froude* number is 0.29. Thus, Δh is expected to be about 4.2 mm, i.e. about 4 % of the flow depth. Since this value is relatively small (Roulund et al. 2005), the rigid lid approximation seems to be acceptable.

3.3. Sub-grid scale model

When using LES, the time-dependent, three-dimensional, spatially-averaged Navier-Stokes equations are solved. In this method, the largest scales are resolved numerically on the mesh, while the unresolved scales must be modeled with a sub-grid scale model. This study adopts the most widely used sub-grid scale model, being the standard Smagorinsky model with a Smagorinsky constant $C_s=0.1$ (Smagorinsky, 1963).

3.4. Numerical solution

The PISO solver was used, since it is the most suitable one for turbulent flows of incompressible fluids (Singh 2004). Both skewness and neighbor correction values were set to 1. Discretization in space and time are second order accurate. A constant time step $\Delta t = 1 \times 10^{-3}$ s was chosen (regarding $\Delta t/T \ll 1$ and after conducting several sensitive analysis). The maximum number of iterations per time-step was 20.

Simulations were carried out on the supercomputer platform of Ghent University. The residual values were controlled and kept below the recommended values for convergence (Kulkarni and Moeykens 2005). After a period of $100T$, a quasi-steady vortex shedding was established.

3.5. Model verification

During the simulations, the residuals value were recorded and kept under the values recommended by Ansys Fluent Theory Guide. After trying several meshes and model parameters, the model described above was found to (largely) fulfill two important criteria. The first criterion is related to the use of the standard wall function and requires the dimensionless wall distance y^+ of the first cells near solid walls to be within the range of $30 \leq y^+ \leq 500$ (Keylock et al. 2012). This condition was verified in several locations of the computation domain, with a special look to the cells near the pier and the bed.

The second criterion requires a LES simulation to have at least 80 % of the turbulent kinetic energy being resolved by the mesh (Pope 2004). Not all parts of the mesh meet this criterion (see Figure 9, obtained by the approach described in Coussement et al. 2012). In the region around the pier, however, the second criterion is largely met.

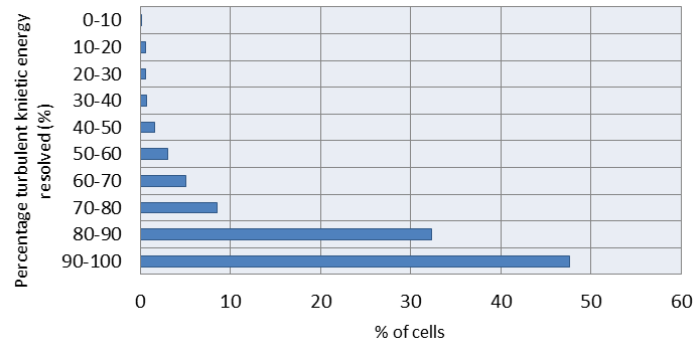


Figure 9. Percentage of turbulent kinetic energy resolved on the mesh

4. RESULTS AND DISCUSSION

4.1. Drag force on the pier

Figure 10 presents the variation in time of the drag coefficient for the entire pier during a period of $60T$. Note that the drag coefficient is calculated automatically by *Fluent* by integrating the instantaneous pressures and shear stresses on the entire pier surface. The drag coefficient is found to oscillate around a mean value (0.602). The irregularities observed in the behavior of the drag coefficient, and thus the drag force, might be explained by the unstable three-dimensional breakup of the vortices, as other studies report (Lysenko et al. 2012). Note that the time-averaged value of the drag coefficient (0.602) is somewhat lower than the value according to the literature (0.683), which was derived in Section 2. The latter value, however, assumes an infinitely long cylinder (with a uniform approaching flow over the depth).

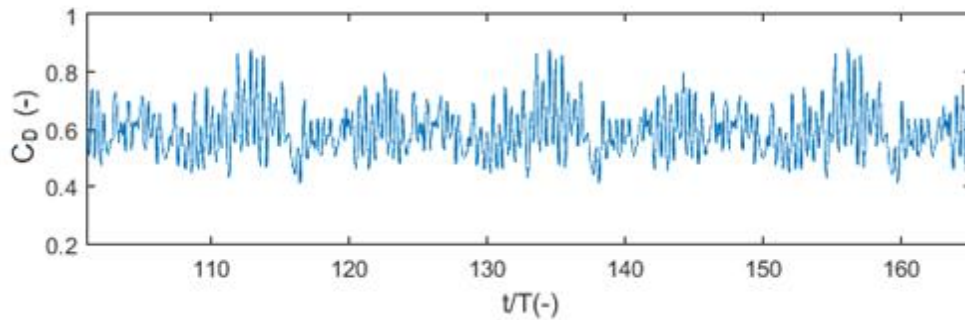


Figure 10. Time evolution of numerically predicted drag coefficient for the entire pier

To quantify the vortex shedding frequency – which is half the value of the drag coefficient oscillations (Blevins 1999) – a Fourier analysis was carried out, resulting in a main frequency of approximately 2.20 Hz (Figure 11). Therefore, the vortices detach themselves from the pier at a frequency of 1.10 Hz. This corresponds to a *Strouhal* number (Equation 1) of 0.19, a value relatively close to the one expected from the literature (0.20, see Section 2).

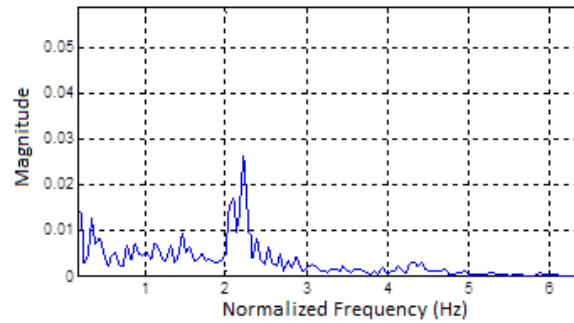


Figure 11. Spectrum of frequencies of the numerically predicted drag coefficient of the entire pier (FFT analysis)

4.2. Velocity fields around the cylindrical pier

The turbulent flow features around a cylinder are vastly documented in the literature. To validate the numerical model results, however, first the available experimental data for this particular flow configuration, will be used. In Figure 12, the velocity profiles $10D$ upstream of the cylindrical pier in the symmetry plane (i.e. point E in Figure 7) are compared ($R^2=0.89$).

Note that the PIV data of the approaching flow are used as inlet boundary condition. Around 3 meters ($62D$) downstream of the inlet, i.e. at point E, the numerical and experimental profiles still match reasonably well, with some discrepancies near the bed (specifying inlet boundary conditions in a LES model is particularly difficult (Zhiyin 2014)). Moreover, it seems that the rigid lid approach does not affect the velocity profile too much, near the upper boundary.

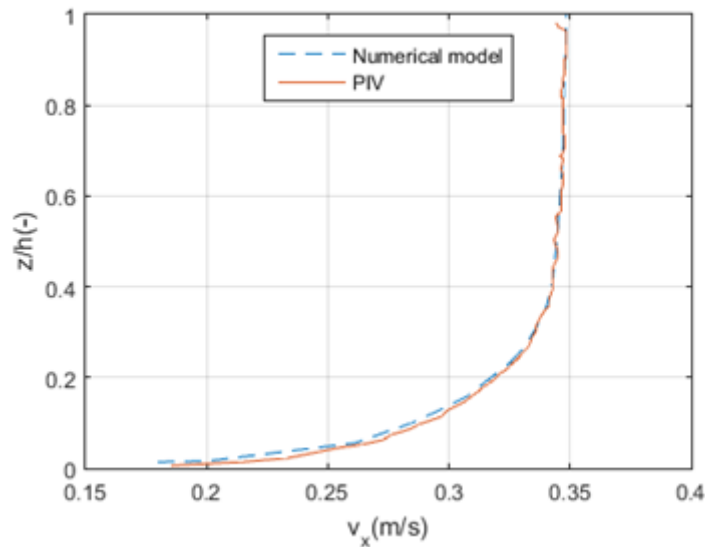


Figure 12. Comparison of measured and numerically predicted approaching velocity profiles in point E of Figure 7 ($10D$ upstream of the cylinder in symmetry plane)

A map of an instantaneous velocity field is presented in Figure 13, for the zone near the bed, upstream of the cylinder. The presence of the horseshoe vortex system and the downflow is evident and the qualitative comparison with the PIV results is satisfactory (see Figure 11 of Nogueira et al. 2008).

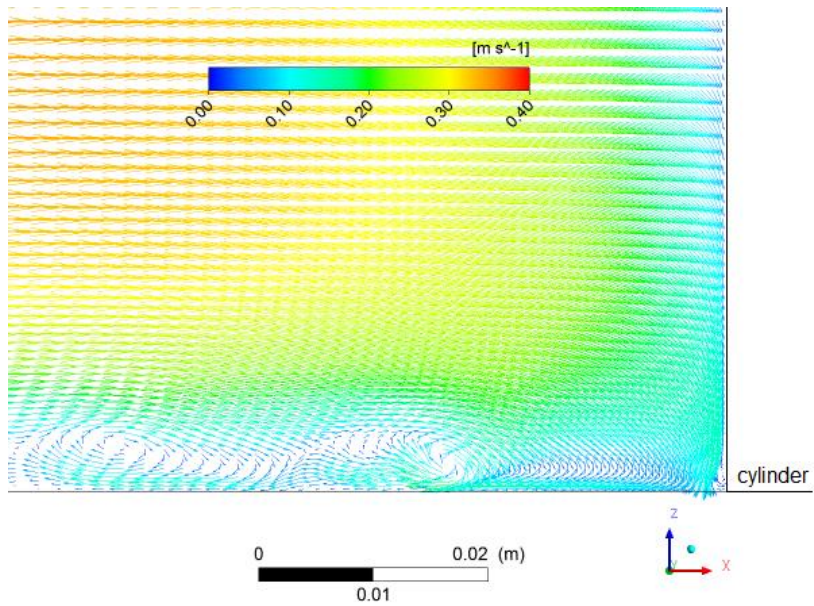


Figure 13. Numerically predicted instantaneous velocity field (near the bed, upstream of the pier) with vectors with colours according to the magnitude (m/s)

In plan view, numerically predicted instantaneous velocity magnitudes around the pier are shown in Figure 14 (at $z/h = 0.5$) and in Figure 15 (at $z/h = 0.01$). In both figures there is a clear influence of the vortex shedding, since the velocities occur asymmetrically in the two distinct instants in time and the individual vortices are perceptible.

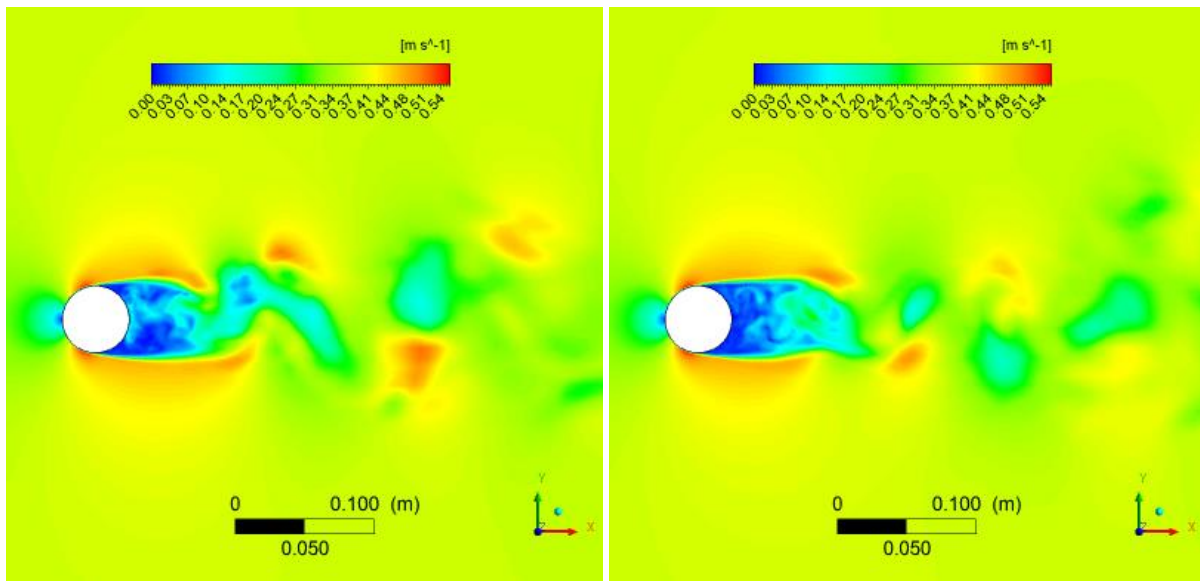


Figure 14. Numerically predicted instantaneous velocity magnitudes in plane $z/h = 0.5$ at two instances in time: $t/T = 150$ (left panel) and $t/T = 155$ (right panel)

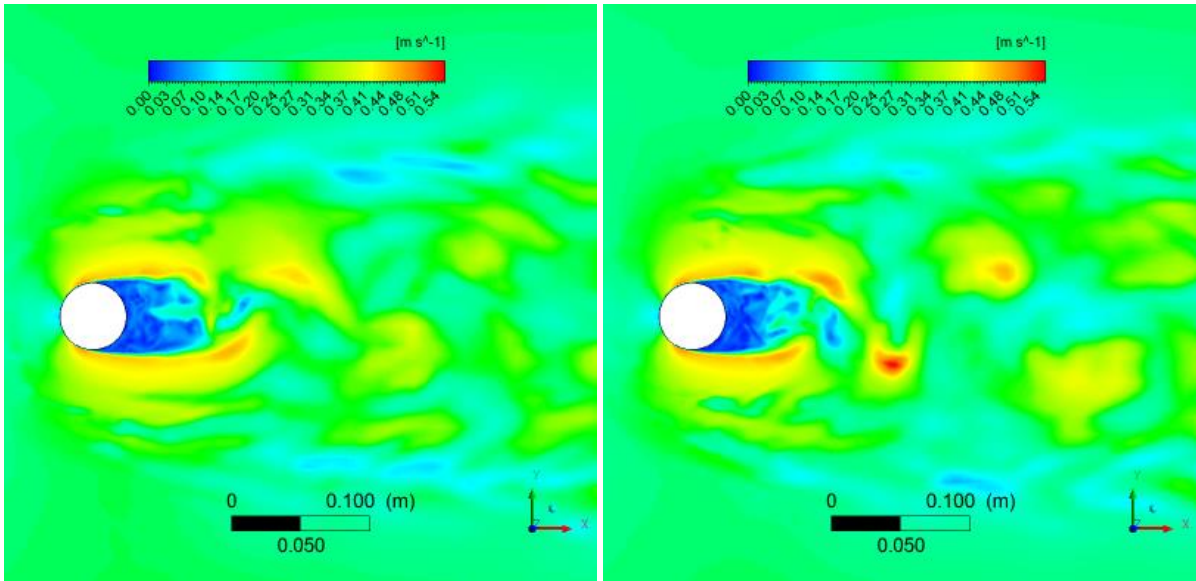


Figure 15. Numerically predicted instantaneous velocity magnitudes in plane $z/h = 0$. at two instances in time: $t/T = 150$ (left panel) and $t/T = 155$ (right panel)

In Figure 16 the velocity in point 1 is presented for a duration of $2T$. The chosen (small) window of time is intended to be able to illustrate the effect of alternating vortices (higher amplitudes) as well as the effect of the smaller turbulence scales (minor variations). However, there is no clear dominant frequency, perhaps due to the location of the chosen point.

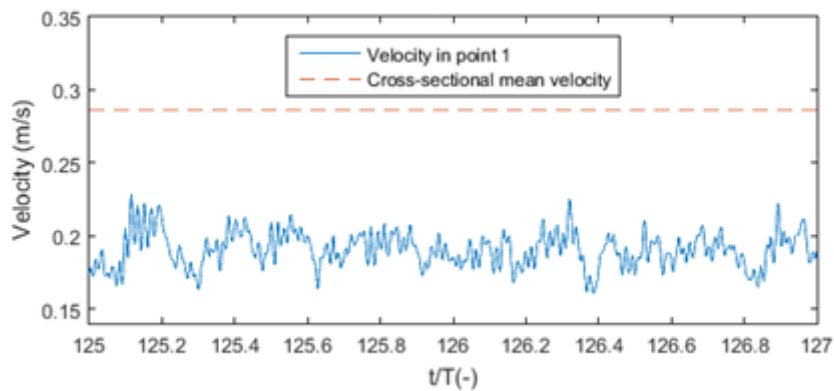


Figure 16. Numerically predicted velocity magnitude at half-height in point 1 (marked in Figure 17)

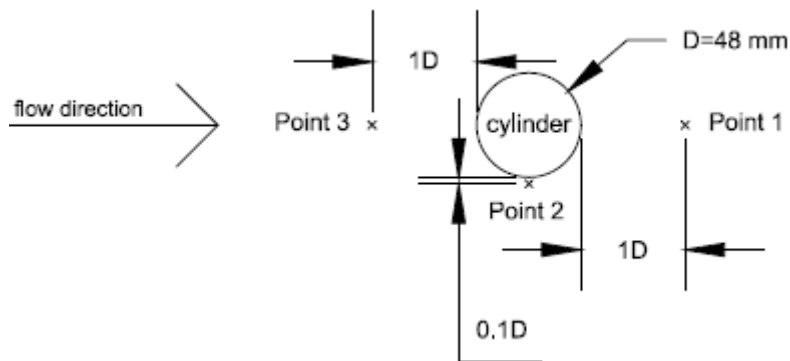


Figure 17. Schematic description (plan view) of the discrete points used to investigate time series of velocity magnitude and bed shear stress. Points 1, 2 and 3 are at $z/h = 0.5$ (half-height), $z/h = 0$ (bed) and $z/h = 0.1$ (near bed), respectively.

Analysis of the velocity magnitude time series in a near-bed point upstream of the pier (point 3 of Figure 17) does not reveal a distinct dominant frequency, suggesting that the horseshoe vortex system has a complex dynamic behaviour.

4.3. Bed shear stress

The flow deflected by the pier induces increased bed shear stresses, capable of moving bed particles, with the higher values in the side close to the pier. Figure 18 shows the temporal evolution of the bed shear stress in point 2 (at the side of the pier, see Figure 17), demonstrating that the critical shear stress for the median diameter of the bed material in the experiments (0.48 Pa, based on the Shields diagram) is often exceeded.

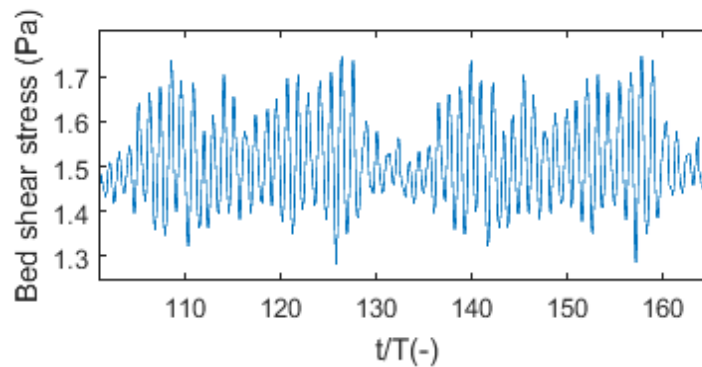


Figure 18. Numerically predicted bed shear stress in point 2 (marked in Figure 17)

Figure 19 shows the shear stress distribution in the vicinity of the pier, highlighting the fact that the highest values are localized on the sides (such as point 2) and in the wake of the pier, possibly associated with the inception of scour.

Nogueira et al. (2008) did not only study the flow around a pier mounted on a flat, non-movable bed (i.e. the flow configuration that is simulated in the present paper), but they also studied the scour around the pier mounted in a movable bed. In Figure 20, the bed after 5 minutes of scour is presented. Note the similarities between the bed shear stress as predicted by the present numerical model and the scour pattern found in the lab experiments.

As literature suggests (Majeed et al. 2015; Guney and Turkben 2015; Ramos et al. 2015), the maximum scour depth during the initial scouring phase in a flume test of this type is not upstream of the pier (i.e. where the equilibrium scour depth is located), but rather at the lateral sides of the cylinder. Note that the bed shear stress patterns predicted in the simulation (which is representative for the initial phase of the scouring process) indeed are in accordance with the observations reported in literature.

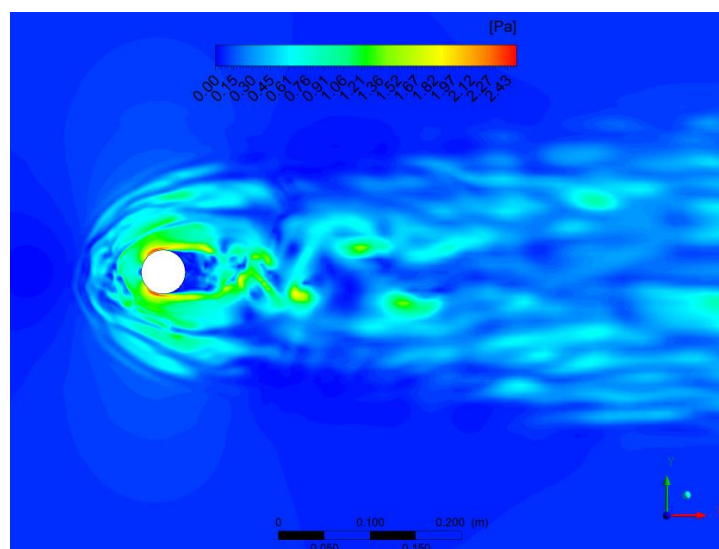


Figure 19. Numerically predicted instantaneous bed shear stress (Pa) around the cylindrical pier

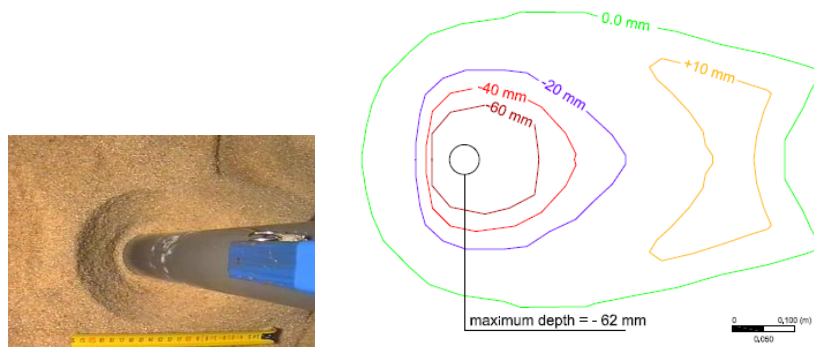


Figure 20. Scoured bed after 5 minutes of flow in movable bed experiments (Nogueira et al. 2008) and contour lines of the corresponding bed level (obtained by P.X. Ramos by means of photogrammetry)

5. CONCLUSIONS

In the present work, an eddy-resolving numerical model based upon the Large Eddy Simulation approach has been set up for predicting the three-dimensional flow around a cylindrical pier, mounted on a flat and fixed bed. This turbulent flow ($Re_D = 1.37 \times 10^4$) configuration was studied earlier experimentally by Nogueira et al. (2008), allowing a partial validation of the numerical results. Since no PIV data are available in the lee side of the cylinder, other validation data from the literature were used as well.

The numerical simulation has confirmed the presence and complex dynamics of the horseshoe vortex system at the upstream side of the cylinder, as was measured by Nogueira et al. (2008). Similarly, the numerical model predicted the vortex shedding in the wake of the cylinder, with a main frequency (and corresponding Strouhal number 0.19) that is very close to value (0.20) in the literature. The mean drag coefficient for the entire pier (0.602) is somewhat lower than the value (0.683) derived from the literature on infinitely long cylinders (i.e. flow configurations with an approaching flow that is uniform over the flow depth). The numerical model confirms the instantaneous drag coefficient (of the entire pier) to oscillate around the mean value, as was reported in the literature.

Since no PIV data are available close to the downstream half of the pier surface, neither in the wake of the pier, no further direct validation of the numerical predictions is possible based upon the data set of Nogueira et al. (2008). An indirect validation of the numerical model is, however, possible based upon the predicted bed shear stresses around the pier. The latter turn out to be higher than the critical value according to the Shields diagram for the bed material used in the experiments, in agreement with the fact that scour was initiated in the experiments. Moreover, the predicted extent of the zone in which the bed shear stress exceeds the critical value, agrees well with the extent of the scour hole observed in the initial phase of the scouring process during the experiments.

Based on this first validation exercise, which is constrained by the limitations of the available data set, it can be concluded that the numerical model is capable of predicting the flow structures well, at least in a qualitative way. However, to enable a further (quantitative) validation of the numerical model, it is advocated to extend the experimental data set. These efforts are needed before the numerical tool is adapted to study the further phases of the scouring process around a cylindrical (or even a geometrically more complex) bridge pier. Currently, both in Ghent University and University of Porto, research on this topic is being carried out, namely regarding complex piers (structure with group of cylinders, a cap and a column) and efforts are being made to implement VoF (Volum of Fluid) in the present numerical model, enabling the study of the phenomena at higher Froude numbers.

6. ACKNOWLEDGEMENTS

The work in this paper has been supported by the European Regional Development Fund (FEDER) through the funds of Competitiveness Factors Operational Programme (COMPETE), the Portuguese Foundation for Science and Technology (FCT) under the project 'Numerical and experimental study of the flow around complex bridge piers' (Ref. FCT EXPL/ECM-HID/1663/2013) and by the Hydraulics Laboratory (Dep. of Civil Engineering) of Ghent University. The authors would like to gratefully mention the contributions of Helena Nogueira and Stéphan Creëlle.

7. REFERENCES

- Beaudan, P. and Moin, P. (1994). Numerical experiments on the flow past a circular cylinder at sub-critical Reynolds number. Technical Report, CTR Annual Research Briefs, NASA Ames/Stanford University.
- Blevins, R. (1990). Flow Induced Vibrations, Krieger Publishing Co., Florida.
- Breuer, A. (1998). Numerical and modeling influences on large eddy simulations for the flow past a circular cylinder. *International. J. Heat and Fluid Flow*, 19, 512-521.
- Catalano, P. Wang, M., Iaccarino, G. and Moin, P. (2003). Numerical simulation of the flow around a circular cylinder at high Reynolds numbers. *Int. J. Heat and Fluid Flow*, 24, 463-469.
- Coussement, A., Gicquel, O. and Degrez, G. (2012). Large eddy simulation of a pulsed jet in cross-flow. *J. Fluid Mech.*, 695, 1-34.
- Ferziger, J.H. and Peric, M. (2002). Computational Methods for Fluid Dynamics, 3rd Edition. Springer, Berlin.
- Fluent theory guide, version 15 (2013), ANSYS, Inc., PA, USA.
- Franke, J. and Frank, W. (2002) Large eddy simulation of the flow past a circular cylinder at $Re_D=3900$. *J. Wind Eng. and Ind. Aerodyn.*, 90: 1191-1206.
- Guney, M.S. and Turkben, A. B. (2015) Experimental Study of Local Scour around Circular Pier under Hydrographs Succeeding Steady Flow. *E-proceedings of the 36th IAHR World Congress 28 June – 3 July, 2015, The Hague, The Netherlands*.
- Hammil, L. (1999). Bridge Hydraulics, E and F Spon, London and New York.
- Keilock, C. Constantinescu, G. and Hardy, R. (2012). The application of computational fluid dynamics to natural river channels: eddy resolving versus mean flow approaches. *Geomorphology*, 179,1-20.
- Kirkil, G. and Constantinescu, G. (2010). Flow and turbulence structure around an in-stream rectangular cylinder with scour hole. *Water Resources Research*, Vol. 46, W11549.
- Kulkarni, A. & Moeykens, S. (2005). *Flow over a cylinder*. FlowLab 1.2 User's Guide, Fluent Inc. New Hampshire, USA.
- Kuroda M., Tamura T. and Suzukim M. (2007). Applicability of LES to the turbulent wake of a rectangular cylinder-comparison with PIV data. *J. Wind Eng. Ind. Aerodyn.*, 95(9):1242-1258
- Launder, B.E. and Spalding, D.B. (1974). The Numerical Computation of Turbulent Flows. *Computer Methods in Applied Mechanics and Engineering*, 3:269-289.
- Lienhard, J.H. (1966). Synopsis of lift, drag and vortex frequency data for rigid circular cylinders. Technical Extension Service, Washington.
- Lisenko, D. A., Ertervag, I. S. and Rian, K. E. (2012). Large-eddy Simulation of the Flow around a Circular Cylinder at Reynolds Number 3900 using the OpenFOAM toolbox. *Flow Turbulence Combust.*, 89:491-518.

Majeed, H., Wright, N. and Sleight, A. (2015). Large eddy simulations and analysis for bridge scour development. *E-proceedings of the 36th IAHR World Congress 28 June – 3 July, 2015, The Hague, The Netherlands*.

Melville, B. and Coleman, S. (2000). *Bridge Scour*. Water Resources Publications LLC, Colorado, USA.

Moreno M, Maia R, Couto L, Cardoso H. 2012. Evaluation of local scour depth around complex bridge piers. *River Flow – International Conference on Fluvial Hydraulics; San Jose, Costa Rica*.

Murakami, S. and Mochida, A. (1995). On Turbulent Vortex Shedding Flow Past 2D Square Cylinder Predicted by CFD. *J. Wind Eng. Ind. Aerodyn.*, 54: 191.

Nakamura Y., Ohya Y., Ozono S. and Nakayama R. (1996). Experimental and numerical analysis of vortex shedding from elongated rectangular cylinders at low Reynolds numbers 200-103. *J. Wind Eng. Ind. Aerodyn.*, 65(1-3):301-308.

Nogueira, H., Franca, M., Adduce, C. and Ferreira, R. (2008). Bridge piers in mobile beds: visualization and characterization of the surrounding and approaching flows. *Proc. River Flow 2008*, Turkey, 2397-2406.

Pope, S. B. (2004). Ten questions concerning the large-eddy simulation of turbulent flow. *New J. Phys.*, 6.

Ramos, P. X., Bento, A. M., Maia, R. and Pêgo, J. P. (2015). Characterization of the scour cavity evolution around a complex bridge pier. *J. Applied Water Eng. and Research*, DOI: 10.1080/23249676.2015.1090353

Rodi, W., Ferziger, J., Breuer, M. and Pourquie, M. (1997). Status of Large Eddy Simulations: Results of a Workshop. *ASME J. Fluids Eng.*, 119: 248-262.

Roshko, A. (1955). On the wake and drag of bluff bodies. *J. Aero. Sci.* 22, 124-32.

Roulund, A., Sumer, M., Fredsøe, J. and Michelsen, J. (2005). Numerical and experimental investigation of flow and scour around a circular pile. *J. Fluid Mech.*, 534: 351- 401.

Sakamoto, S., Murakami, S., and Mochida, A. (1993). Numerical Study on Flow Past 2D Square Cylinder by Large Eddy Simulation. *J. Wind Eng. Ind. Aerodyn.*, 50, pp. 61-68.

Schanderl, W. and Manhart, M. (2016). Reliability of wall shear stress estimations of the flow around a wall-mounted cylinder. *Computers and Fluids* 128

Shields, A. (1936). Anwendung der Ähnlichkeitsmechanik und der Turbulenzforschung auf die Geschiebebewegung; In Mitteilungen der Preussischen Versuchsanstalt für Wasserbau und Schiffbau, 26.

Smagorinsky, J. (1963). General Circulation Experiments with the Primitive Equations. *Mon. Weather Rev.*, 91, 99-165.

Techet, A. H. (2005). Vortex Induced Vibrations. *MIT OCW*: <http://ocw.mit.edu/courses/mechanical-engineering/2-22-design-principles-for-ocean-vehicles-13-42-spring-2005/readings/lec20_viv1.pdf> (April 25, 2016).

Thwaites, B. (1960). *Incompressible aerodynamics*, University Press, Oxford.

White, F. (2006). *Fluid Mechanics*. 6th edition. McGraw-Hill Companies. South Kingstown, UK.

Yang, K.S., and Ferziger, J. (1993). Large-Eddy Simulation of Turbulent Obstacle Flow Using a Dynamic Subgrid-Scale Model. *AIAA J.*, 31, 1406–1413.

Yulistiyanto, B. Zech, Y. and Graf, W. H. (1998). Flow around a Cylinder: Shallow-Water Modeling with Diffusion-Dispersion. *J. Hydr. Eng.*, 124(4): 419-429.

Zdravkovich, M.M. (1997). Flow around circular cylinders, Vol 1: fundamentals, Oxford University Press, Oxford, New York.

Zhao, W. and Huhe, A. (2006). Large-Eddy simulation of three-dimensional turbulent flow around a circular pier. *J. Hydrodynamics*. 218(6):765-772.

Zhiyin, Y. (2014). Large-eddy simulation: past, present and the future. *Chinese J. Aeronautic*. 28(1):11-24.